Optics Letters

Photonic crystal resonators for inverse-designed multi-dimensional optical interconnects

C. Shirpurkar,[1,5,†] J. Zang,[2,†] K. Y. Yang,[3,†] D. Carlson,[2] S. P Yu,[2] E. Lucas,[2] S. V. Pericherla,[1] J. Yang,[3] M. Guidry,[3] D. Lukin,[3] G. H. Ahn,[3] J. Lu,[3] L. Trask,[1] F. Aflatouni,[4] J. Vučković,[3] S. B. Papp,[2] and P. J. Delfyett[1,6]

[1]CREOL, The College of Optics and Photonics, University of Central Florida, Orlando, Florida, 32816, USA
[2]Time and Frequency Division, National Institute of Standards and Technology, Boulder, Colorado, USA
[3]E.L. Ginzton Laboratory, Stanford University, Stanford, California, USA
[4]Department of Electrical and Systems Engineering, University of Pennsylvania, Philadelphia, Pennsylvania, USA
[5]e-mail: shirpurkar.chinmay@knights.ucf.edu
[6]e-mail: delfyett@creol.ucf.edu
[†]These authors contributed equally to this work.

Received 21 April 2022; revised 10 May 2022; accepted 10 May 2022; posted 11 May 2022; published 9 June 2022

We experimentally demonstrate a 400 Gbit/s optical communication link utilizing wavelength-division multiplexing and mode-division multiplexing for a total of 40 channels. This link utilizes a novel, to the best of our knowledge, 400 GHz frequency comb source based on a chip-scale photonic crystal resonator. Silicon-on-insulator photonic inverse-designed 4 × 4 mode-division multiplexer structures enable a fourfold increase in data capacity. We show less than −10 dBm of optical receiver power for error-free data transmission in 34 out of a total of 40 channels using a PRBS31 pattern.

https://doi.org/10.1364/OL.461272

Technological advancements in the past decade have paved the way toward high-capacity, low-power data transmission using photonic interconnects. One of the most important applications for these interconnects is in data centers, which require the transfer of massive amounts of information between many individual processors and memory. Although purely electrical interconnects can be used for this, the high-frequency capabilities and low losses in electronic–photonic interconnects allow for much higher bandwidth and greater efficiency [1,2]. Data modulation schemes are important as they determine several factors, such as receiver sensitivity, bit error rate, and overall complexity of the system. Coherent modulation schemes can provide extremely high data rates as well as lower receiver sensitivity, but they can also require complex digital signal processing (DSP) and complicated components, such as ultra-narrow linewidth lasers, in-phase/quadrature (IQ) modulators, and coherent receivers [3–7]. Direct direction schemes using such formats as non-return-to-zero (NRZ) or four-level/eight-level pulse amplitude modulation (PAM4/PAM8) have lower speeds than coherent modulation but require simpler components with less demanding DSP at the receiver [8,9]. Considering power and cost requirements, direct detection schemes are more suitable for short intra data-center links. However, as the demand for data rates increases, intensity modulation with direct detection (IM/DD) becomes progressively more challenging. Parallelization can increase data rates drastically while utilizing these low-complexity data modulation formats. The most common method of increasing the number of communication channels is wavelength division multiplexing (WDM). However, this approach is typically limited by the increased complexity required for the design of high optical bandwidth components.

One promising way to increase the number of channels is to increase the dimensionality of multiplexing in the spatial domain. Orthogonal spatial modes in multi-mode optical waveguides can serve as independent communication channels, each of which support an entire WDM link [10,11]. Mode-division multiplexing (MDM) can therefore multiplicatively scale up the bandwidth of the link. Conventional photonic devices are typically simplified geometrical designs based on theoretical derivations and only reveal a small fraction of the vast number of possible designs. Photonic inverse design [12–14] is a computational nanophotonic design approach that uses gradient-based optimization to optimize permittivity distribution for the targeted designs. This method provides an efficient way to explore the full space of possible designs while offering smaller footprints, better efficiencies, and novel functionalities. In this work, we utilize a four-channel inverse-designed mode-division multiplexer along with a 400 GHz microcomb from a normal dispersion photonic crystal resonator (PhCR) to realize a 40-channel link.

The inverse-designed MDM devices are fabricated on a standard silicon-on-insulator platform (silicon thickness: 220 nm). Figure 1 shows a micrograph of the MDM multiplexer/demultiplexer, which has a design area of $6.5 \times 6.5\ \mu m^2$ with a foundry-compatible minimum feature size (80 nm) [15]. The multiplexer routes the fundamental TE_{00} mode of the 500 nm-wide input waveguides to the TE_{00} (channel 1), TE_{20} (channel 2), TE_{30} (channel 3), and TE_{40} (channel 4) modes of the 1800 nm multi-mode waveguide. The demultiplexer after the multi-mode waveguide again converts the higher-order modes

Fig. 1. Micrograph of four-channel back-to-back inverse-designed MDM multiplexer devices.

down to the TE_{00} modes in the four channels. The MDM device used in these experiments is a back-to-back structure using a multi-mode waveguide having less than −18 dBm of modal cross talk for all mode channels. Future testing involves a chip-to-chip link using MDM structures with coupling to multi-mode waveguides via inverse-designed edge couplers or grating couplers [13].

Microresonator-based optical frequency combs have the potential to revolutionize WDM links by replacing laser arrays with low power consumption microcombs. Dark pulse combs formed in normal dispersion microresonators have the advantage of higher energy efficiency and better spectral flatness compared with bright pulse combs in the anomalous dispersion regime. However, phase matching for comb generation is conventionally not possible in normal dispersion resonators. In this work, this is overcome by designing and fabricating edgeless PhCRs [16,17]. The PhCRs are fabricated from a tantalum pentoxide (Ta_2O_5) material platform. A ring waveguide of height 570 nm and width 2100 nm provides normal dispersion at the 1550 nm wavelength with an average intrinsic Q of 2.2×10^6. Their inner wall is modified by an azimuthally uniform sinusoidal nanopatterned oscillation, as shown in the inset of Fig. 2(b). This modulation leads to a photonic bandgap at one of the resonant modes. As a result, it is split into two modes and the mode splitting depends on the amplitude of the nanopatterned modulation. Pumping the lower frequency mode unconditionally satisfies the phase matching condition of the four-wave mixing required for comb initiation in normal dispersion. Further red detuning of the pump laser reveals rich nonlinear dynamics and comb profiles, including dark pulses. The attractive feature of these combs is that they do not require any fast wavelength tuning methods to excite

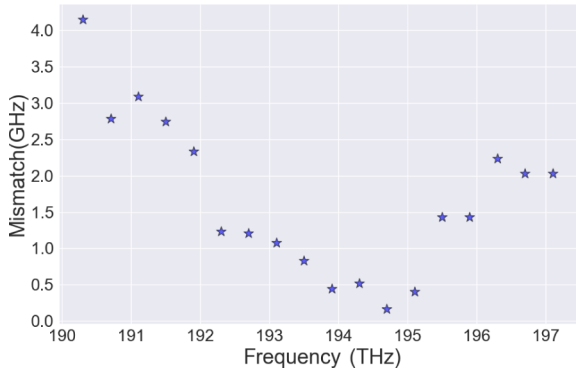

Fig. 3. Comb line frequency versus frequency mismatch between ITU grid frequency and corresponding comb line frequency measured using grating-based optical spectrum analyzer.

low-noise mode-locked comb states, owing to the elimination of Turing patterns and chaotic states [17,18].

In addition to the benefits of comb generation using manual wavelength tuning, the PhCR split modes and free spectral range (FSR) can be tailored precisely to generate combs at the desired wavelength. In these experiments, the generated comb has been designed to match the wavelengths of the International Telecommunication Union (ITU) grid. The WDMs used in the experiments are commercially available, with narrow 3 dB Gaussian passbands of 10 GHz, so it is important that the generated comb lines match these frequencies. The mismatch of the generated comb frequency with respect to its corresponding ITU channel is shown in Fig. 3. The misalignment is lower than 4 GHz, which is well within the bandwidth of the commercial WDM.

Figure 2(a) shows, schematically, all the components in the experimental setup. The comb is generated by pumping the PhCR with a tunable external-cavity diode laser (ECDL). The pump wavelength is controlled and detuned via an external piezo modulation input to the laser. In our experiments, the PhCR rings are designed so that the split-mode is at a wavelength of 1550 nm and require about 18 dBm of pump power on the chip. The output of the comb is then passed through a narrowband fiber Bragg grating that serves to suppress the excess pump power. Figure 2(b) shows the spectrum of the generated comb

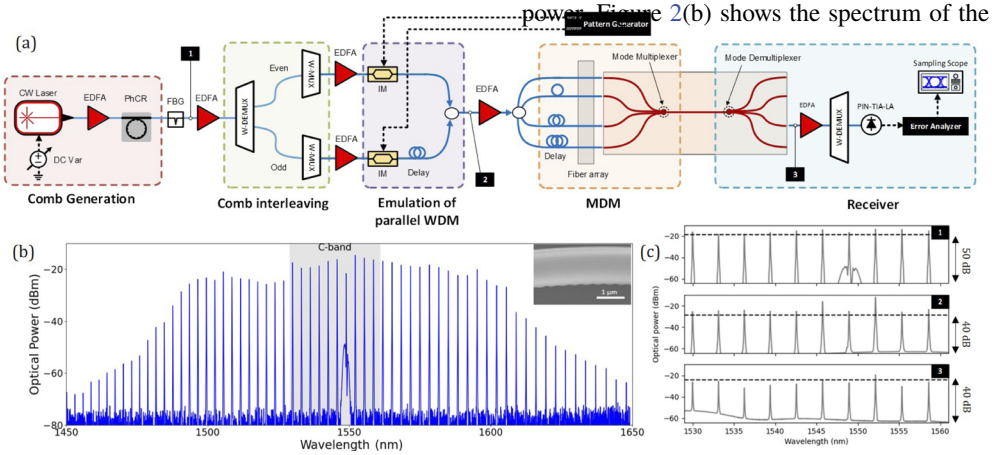

Fig. 2. (a) Experimental setup for WDM–MDM microcomb data transmission. DC Var, variable DC voltage; EDFA, erbium-doped fiber amplifier; FBG, fiber Bragg grating; IM, intensity modulator; PhCR, photonic crystal ring resonator; PIN-TIA-LA, PIN photodiode transimpedance amplifier and limiting amplifier. (b) Optical spectrum of 400 GHz FSR PhCR comb with C-band highlighted (inset: scanning electron micrograph of sinusoidal nanopattern on inner edge of ring). (c) Optical spectrum of PhCR comb pulse in C-band range at various points in the setup; 1, 2, 3 as highlighted in (a). Spectrum 3 is taken for MDM CH 3.

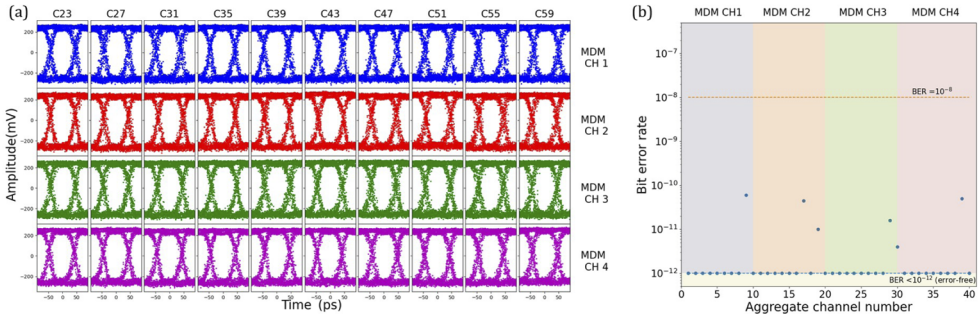

Fig. 4. (a) 10 Gbit/s eye diagrams for all channels in the link at −10 dBm optical received power. (b) Measured BERs (10^{12} bits compared) of the transmitted data channels at −10 dBm optical received power: 34 channels have BER$<10^{-12}$. Aggregate channel numbers go from C23 to C59 (left to right) for each of the highlighted MDM channel sections.

with the pump suppressed. The generated comb has a relatively flat spectrum with lines having sufficient power to be used for data transmission over a 100 nm bandwidth. In this work, we only use a part of the C-band (C23-C59), highlighted in gray in Fig. 2(b), which gives us 10 WDM channels. The transmitted comb is then amplified and demultiplexed using a commercial 100 GHz ITU grid based dense wavelength division multiplexer (DWDM). To emulate simultaneous data transmission through all channels, we recombine "even" and "odd" carrier channels using another multiplexer. Each channel is separately amplified and passed through two lithium-niobate electro-optic intensity modulators, which are driven by a PRBS31 NRZ pattern generator at a rate of 10 Gbit/s. The data channels are decorrelated with a delay of approximately 5000 symbols. We recombine the odd and even sets of data, amplify them, and split the power into four different outputs, which are sent simultaneously into the MDM channels using a v-groove fiber array. Mode channels 2–4 have a delay of 50, 100, and 200 symbols with respect to mode channel 1. The output from each of the MDM channels is selected one at a time using a lensed fiber. The output is then amplified and sent through another wavelength demultiplexer, where the signal is detected using an 8 GHz optical photoreceiver with an integrated transimpedance amplifier (TIA) and an output limiting amplifier. The ten WDM channels and four MDM channels, at a speed of 10 Gbit/s per channel totalize a data transmission rate of 400 Gbit/s.

It is important to record the optical spectrum of the comb at various points in the setup to keep track of wavelength and polarization-dependent gains or losses. The EDFAs in the system can have different gains for different wavelengths, owing to varying input power per wavelength channel, as well as non-uniform gain across the C-band. The intensity modulators have polarization-dependent losses since different wavelength channels need a different input polarization for optimum performance. Figure 2(c) shows the optical spectrum in the C-band at three different points, as marked by Fig. 2(a). The comb lines have an optical signal to noise ratio (OSNR) of greater than 50 dB immediately out of the PhCR (limited by the noise floor of the optical spectrum analyzer, ∼ −80 dBm), which degrades to approximately 40 dB before the input to the MDM device. After the MDM device (for MDM CH 3), the shorter wavelength channels have a reduced OSNR of ∼20 dB, while the higher wavelength channels are relatively unaffected.

The output limiting amplifier is a high-speed, high-sensitivity digital device, which quantizes the analog signal coming from the TIA and returns a well-defined level of "1" or "0." The

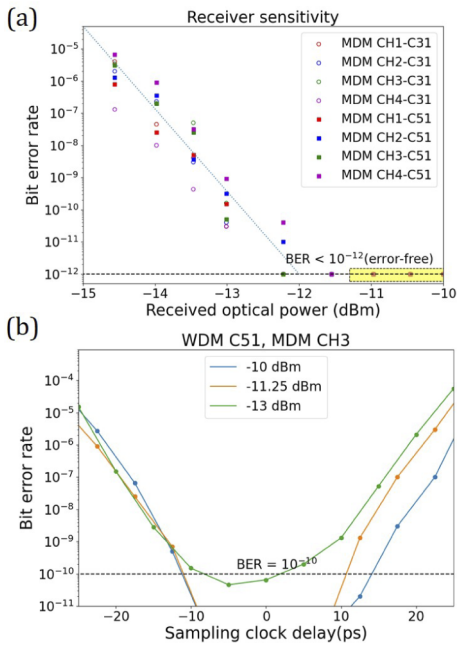

Fig. 5. (a) Receiver sensitivity: BER versus optical power for C31 and C51 across all MDM channels. (b) Bathtub curve for C51 MDM CH 3.

output signal from the PIN-TIA-LA is input into an error analyzer to determine bit error rates (BERs). The eye diagrams for a received optical power of −10 dBm are shown in Fig. 4(a) and have an eye opening of 500 mVpp. The BERs at an optical receiver power of −10 dBm for each channel are given in Fig. 4(b). We can see that 34 out of 40 channels are error-free (BER$<10^{-12}$), with the highest BER being 10^{-10}. Figure 5(a) shows the receiver sensitivity curve for receiver powers from 30 to 100 μW. Optical powers below 30 μW on the receiver result in a loss of synchronization between the pattern generator and the error analyzer. To measure the sampling window for error-free transmission, we also record the "bathtub curve" for WDM C51, MDM CH 3 at different optical receiver powers, as shown in Fig. 5(b). We can see that, at powers of 75 μW and above, we have a 20 ps sampling window for error-free transmission.

In summary, we have demonstrated a WDM–MDM optical communication scheme using novel integrated photonic devices. With an inverse-designed silicon MDM device and chip-scale

PhCRs, we multiplex four spatial modes and ten wavelength channels covering the C-band to achieve error-free (BER$<10^{-12}$) data transmission in 34 out of 40 channels at −10 dBm optical receiver power for a 340 Gbit/s error-free transmission with a total of 400 Gbit/s across 40 channels. The work presented here opens a path toward massively parallel high-capacity integrated photonic interconnects. Further improvements would involve using PhCRs of 200 GHz FSR or higher channel MDM structures. Greater utilization of the comb bandwidth, such as including the L-band, would also greatly increase data rates. Further integration of such components as WDMs and lasers can lead to the next generation of optical interconnects in data-center networks. Further chip-to-chip testing of the MDM device structures using multi-mode fiber is also required to test effects of cross talk and environment-induced noise for short multi-mode communication links.

Funding. Defense Advanced Research Projects Agency (HR0011-19-2-0016); National Science Foundation (IUCRC 2052701).

Acknowledgment. We thank Dr. Guifang Li and Mr. Dhruvkumar Desai at the Optical Fiber Communications Group at CREOL, The College of Optics and Photonics, for providing the bit error rate testing equipment used in these experiments.

Disclosures. The authors declare no conflicts of interest.

Data availability. Data underlying the results presented in this paper are not publicly available at this time but may be obtained from the authors upon reasonable request.

REFERENCES

1. D. A. Miller, in *Integrated Photonics Research, Silicon and Nanophotonics and Photonics in Switching*, OSA Technical Digest (Optica Publishing Group, 2010), paper PMB3 .
2. D. A. Miller, J. Lightwave Technol. **35**, 346 (2017).
3. J. K. Perin, A. Shastri, and J. M. Kahn, J. Lightwave Technol. **39**, 730 (2021).
4. J. Pfeifle, V. Brasch, M. Lauermann, Y. Yu, D. Wegner, T. Herr, K. Hartinger, P. Schindler, J. Li, D. Hillerkuss, R. Schmogrow, C. Weimann, R. Holzwarth, W. Freude, J. Leuthold, T. J. Kippenberg, and C. Koos, Nat. Photonics **8**, 375 (2014).
5. A. Fülöp, M. Mazur, A. Lorences-Riesgo, Ó. B. Helgason, P. H. Wang, Y. Xuan, D. E. Leaird, M. Qi, P. A. Andrekson, A. M. Weiner, and V. Torres-Company, Nat. Commun. **9**, 1598 (2018).
6. P. Marin-Palomo, J. N. Kemal, M. Karpov, A. Kordts, J. Pfeifle, M. H. Pfeiffer, P. Trocha, S. Wolf, V. Brasch, M. H. Anderson, R. Rosenberger, K. Vijayan, W. Freude, T. J. Kippenberg, and C. Koos, Nature **546**, 274 (2017).
7. K. Kikuchi, J. Lightwave Technol. **34**, 157 (2016).
8. K. Szczerba, P. Westbergh, J. Karout, J. S. Gustavsson, Å. Haglund, M. Karlsson, P. A. Andrekson, E. Agrell, and A. Larsson, J. Opt. Commun. Netw. **4**, 885 (2012).
9. R. Nagarajan, M. Filer, Y. Fu, M. Kato, T. Rope, and J. Stewart, J. Opt. Commun. Netw. **10**, B25 (2018).
10. J. M. Kahn and D. A. Miller, Nat. Photonics **11**, 5 (2017).
11. D. J. Richardson, J. M. Fini, and L. E. Nelson, Nat. Photonics **7**, 354 (2013).
12. S. Molesky, Z. Lin, A. Y. Piggott, W. Jin, J. Vučković, and A. W. Rodriguez, Nat. Photonics **12**, 659 (2018).
13. K. Y. Yang, A. D. White, and F. Ashtiani, *et al.*, "Inverse-designed multi dimensional silicon photonic transmitters," arXiv2103.14139, (2021).
14. A. Y. Piggott, J. Lu, K. G. Lagoudakis, J. Petykiewicz, T. M. Babinec, and J. Vučković, Nat. Photonics **9**, 374 (2015).
15. M. Rakowski, C. Meagher, and K. Nummy, *et al.*, in *Optical Fiber Communication Conference (OFC) 2020*, OSA Technical Digest, (Optica Publishing Group, 2020), paper T3H.3.
16. S.-P. Yu, E. Lucas, J. Zang, and S. B. Papp, "A continuum of bright and dark pulse states in a photonic-crystal resonator," arXiv 2109.01280 (2021).
17. S. P. Yu, D. C. Cole, H. Jung, G. T. Moille, K. Srinivasan, and S. B. Papp, Nat. Photonics **15**, 461 (2021).
18. T. C. Briles, S. P. Yu, T. E. Drake, J. R. Stone, and S. B. Papp, Phys. Rev. Appl. **14**, 014006 (2020).